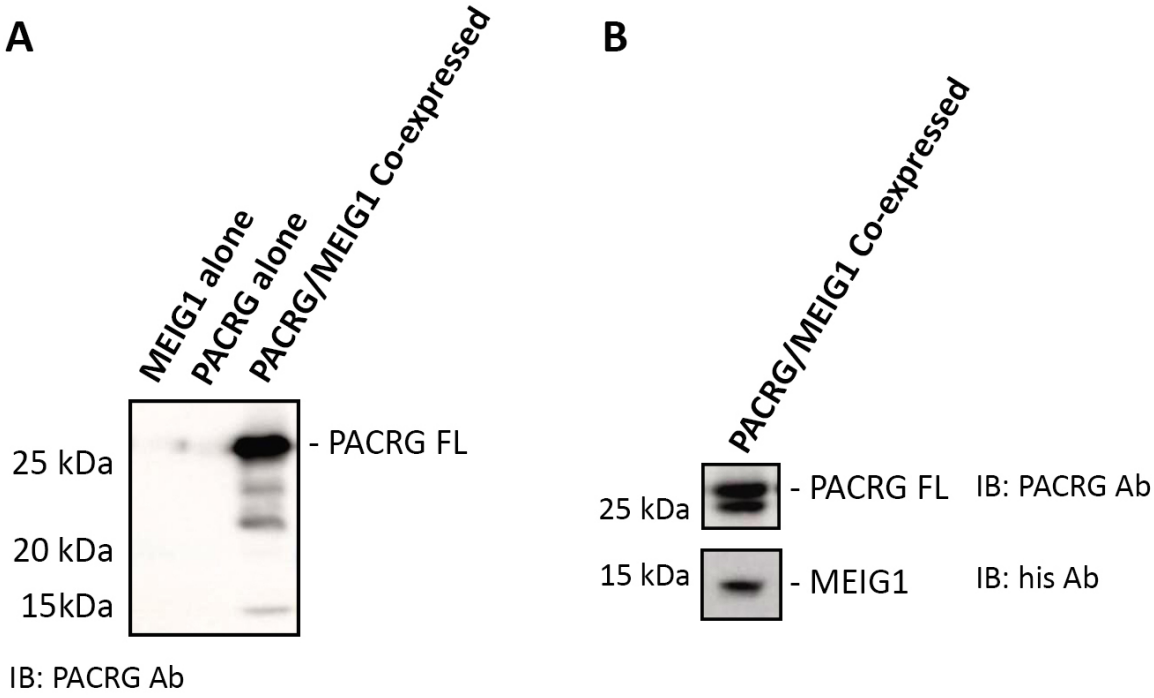

Supplemental Figure S1. $PACRG_{FL}$:MEIG1 co-expression in *E. coli*, related to Figure 1. (A) Cells expressing MEIG1 or PACRG alone showed little to no signal at 29 kDa, $PACRG_{FL}$ expected size, when blotted against PACRG. When PACRG was co-expressed with MEIG1, proteins levels significantly increased. Lysates were normalized by total protein concentration. **(B)** Cell lysates were blotted against PACRG and the his-tag on MEIG1 to indicate that both proteins were indeed expressed. Immunoblotting was performed with PBS with 0.1% Tween 20 with either PACRG mouse monoclonal antibody (1:2000, Santa Cruz Biotechnology, Inc.) or His-tag polyclonal rabbit antibody (1:2000, Cell Signaling Technology) in 15 mL of PBST with 2% bovine serum albumin (BSA), shaking over night at 4°C.

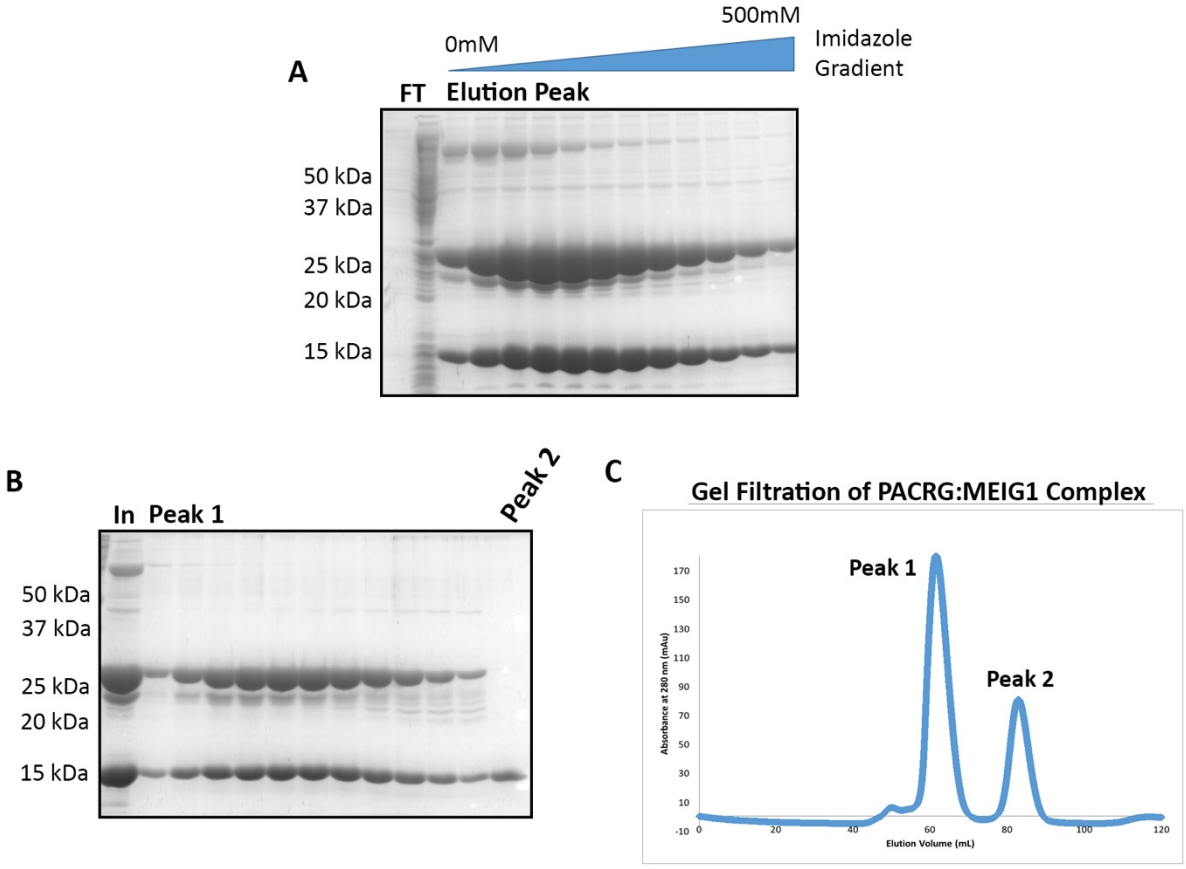

Supplemental Figure S2. **Purification of co-expressed PACRG$_{FL}$:MEIG1, related to Figure 1. (A)**. A richer media, TB, was used for E. coli growth and protein production followed by Ni-NTA gradient purification. The flow-through removed many impurities. An imidazole gradient (0-500 mM, blue bar) was used to separate the complex from *E. coli* proteins that bound to the column non-specifically. The complex was expressed in large amounts, PACRG$_{FL}$ at 29 kDa and MEIG1 at 16 kDa. The *E. coli* Lac Operon Repressor protein, large band above 50 kDa, was still present. **(B)**. Gel filtration was performed on the elutions from the Ni-NTA purification to remove large impurities like the Lac Operon Repressor. SDS-PAGE of gel filtration peaks. Peak1 corresponded to the complex, it was relatively pure enough to stop at this purification step. Peak 2 corresponded to free MEIG1 that did not bind to PACRG$_{FL}$. **(C)** Chromatogram of gel filtration, input was the elution fractions from Ni-NTA purification. The gel filtration separated the proteins successfully, the shoulder to the left of peak 1 corresponds to the Lac Operon Repressor. FT: flow through, In: input.

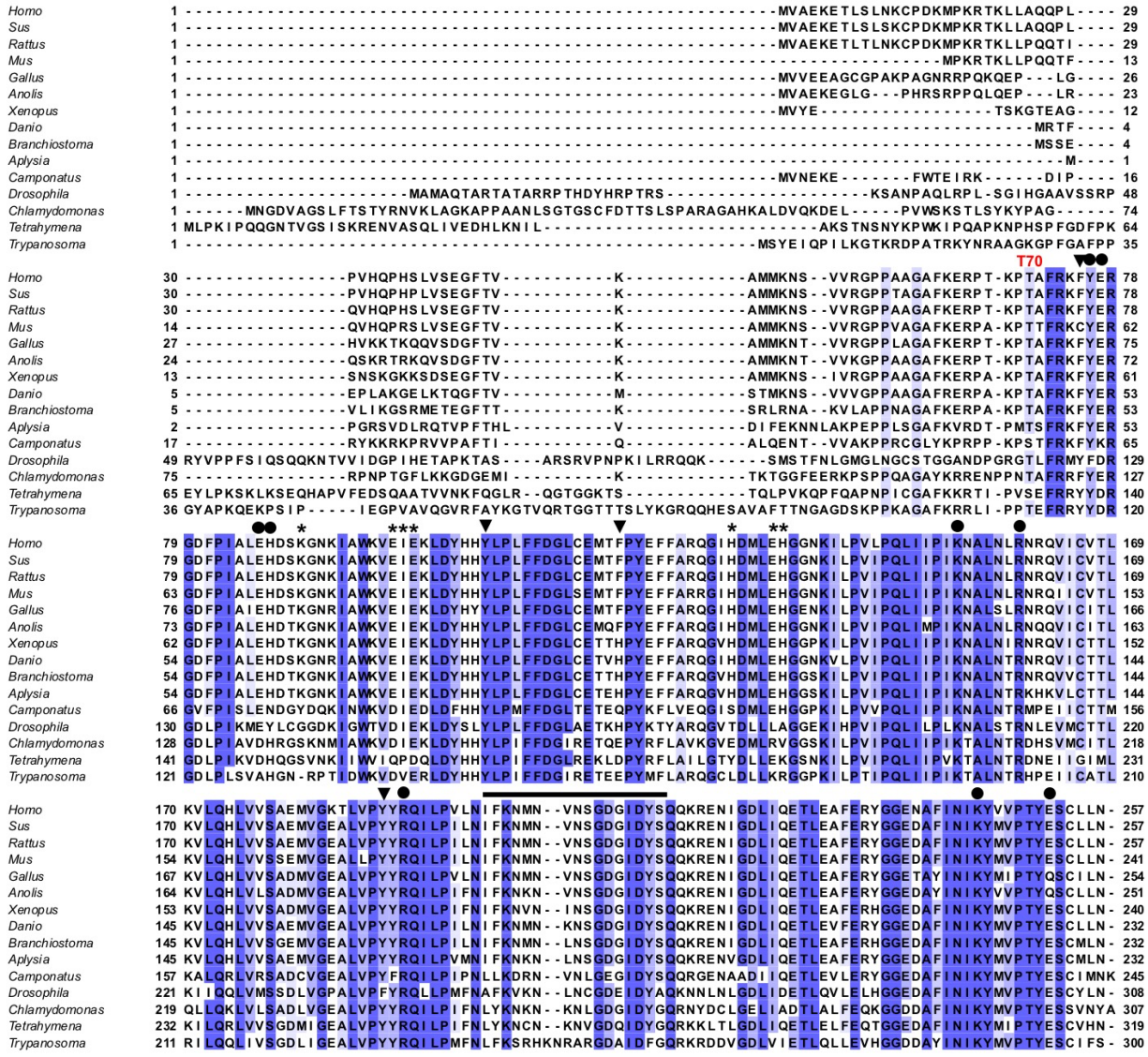

Supplemental Figure S3. **Sequence alignment of PACRG protein orthologs from different species, related to Figure 1.** PACRG N-terminal is highly variable across species, whereas the C-terminus is more conserved. Deletion constructs were made by deleting amino acids 1-69 (a.a. Thr70 labeled in red) in human PACRG. Positions labeled with black arrows indicate site where p-iodo-L-phenylalanine was incorporated for phasing. Asterisks indicate residues important for binding MEIG1. Black circles highlight residues that interact with tubulin in the axonemal doublet tubule structure.

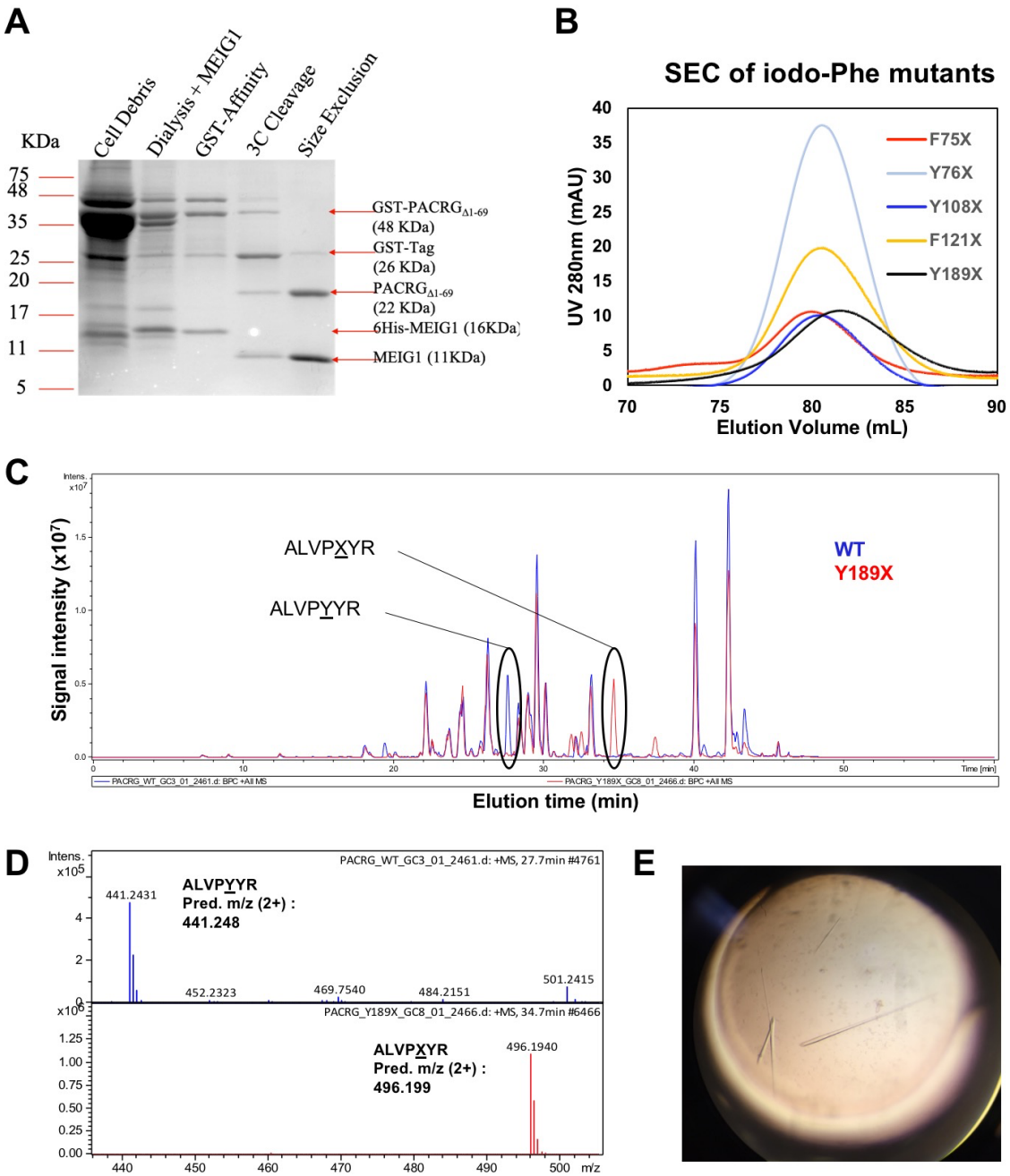

Supplemental Figure S4. **Purification of *p*-iodo-*L*-phenylalanine mutants of PACRG$^{\Delta 1\text{-}69}$ bound to MEIG1, related to Figure 1. (A)** Fractions from the Y189X PACRG $_{\Delta 1\text{-}69}$ mutant inclusion body purification migrated on SDS-PAGE gel and stained with Coomassie Brilliant Blue. The fractions consisted of protein from the cell debris collected after removing the cleared lysate (Cell Debris), after dialysis and addition of MEIG1 (Dialysis+MEIG1), after GST-affinity chromatography (GST-Affinity), following overnight 3C protease cleavage (3C cleavage), and after size-exclusion chromatography (Superdex 75). **(B).** UV 280 nm intensity for all eluted mutants on size-exclusion chromatography. **(C)** Extracted ion chromatograms of tryptic peptides from the wild type (WT) and Y189X mutant ofPACRG$^{\Delta 1\text{-}69}$ bound to MEIG1. All peptides are identical except the peptide spanning amino acids 185-191, which contains iodo-phenylalanine at position 189. **(D)** The precursor spectra indicate the mass shift induced by the incorporation of iodo-phenylalanine. **(E)** Crystals of the MEIG1:PACRG$^{\Delta 1\text{-}69}$ Y189X complex.

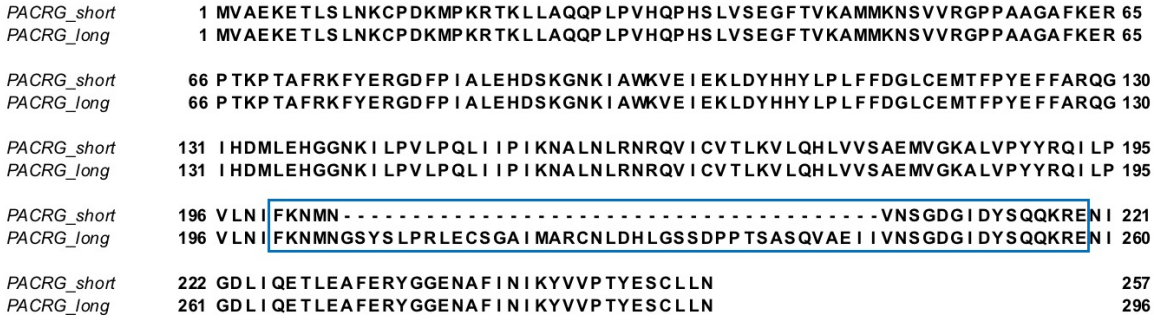

Supplemental Figure S5. **Sequence alignment of PACRG isoforms, related to Figure 1.** The disordered loop in between α6 and α7 in the crystal structure of the short isoform of PACRG is highlighted with a blue box.

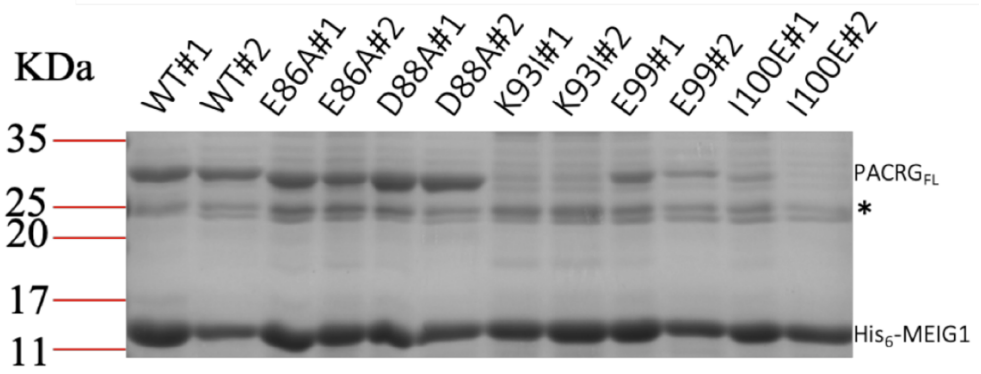

Supplemental Figure S6. **Interaction assay for the binding of PACRG mutants to His$_6$-MEIG1, related to Figure 2.** WT or mutants PACRG^{FL} were expressed with His$_6$-MEIG1 from a single pRSF-DUET plasmid. Following expression in E.coli, the cell lysate was incubated with Co-NTA affinity resin to pull-down on His$_6$-MEIG1. The eluate was loaded directly on SDS-PAGE and stained with Coomassie (example shown here). Densitometry was performed on both the PACRGFL and His$_6$-MEIG1 bands to calculate the ratios showed in Figure 2B. Each mutant was tested 4 times independently. The asterisk indicates a contaminant protein co-eluting non-specifically on Co-NTA.

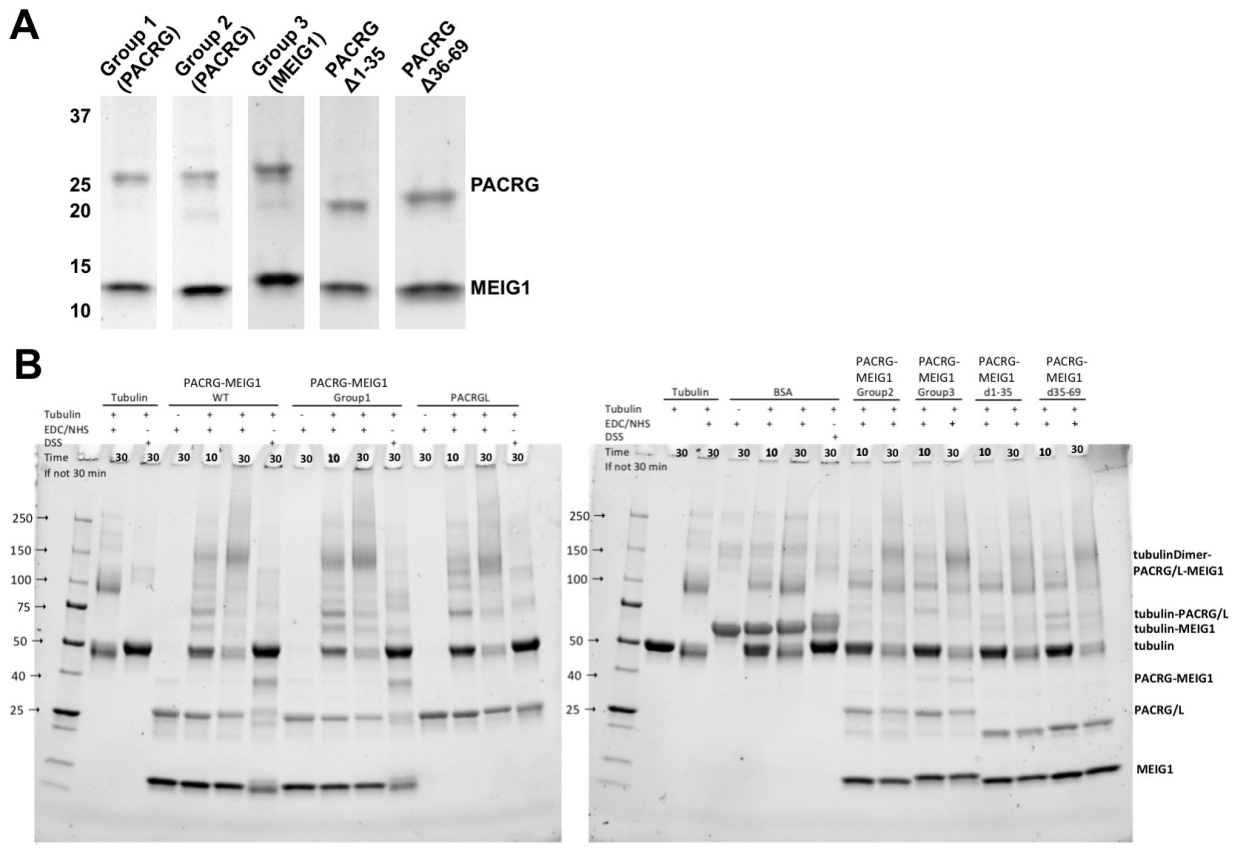

Supplemental Figure S7. **Crosslinking studies show that PACRG:MEIG1 and PACRGL bind to tubulin, related to Figure 4 and 5. (A**) Purification of PACRG:MEIG1 group mutants used in the tubulin recruitment and crosslinking assays. Proteins were purified by affinity chromatography, 3C cleavage and size-exclusion chromatography. Products were resolved on SDS-PAGE and visualized using Bio-rad stain-free UV 4-20% pre-cast gels. Group 1: PACRG Y76F-E77K-E86K-H87A; group 2: PACRG K154E-R160Q-R191E; group 3: MEIG1 H13A-K78A-H81A-K82A-Y86A. **(B)** SDS-PAGE analysis of crosslinking reactions between tubulin (5 μM) and different candidate microtubule-associated proteins (12.5 μM), using either EDC/NHS or DSS as crosslinker (10 and 30 min). Gels were imaged by UV-induced fluorescence (Biorad TGX Stain-Free technology).

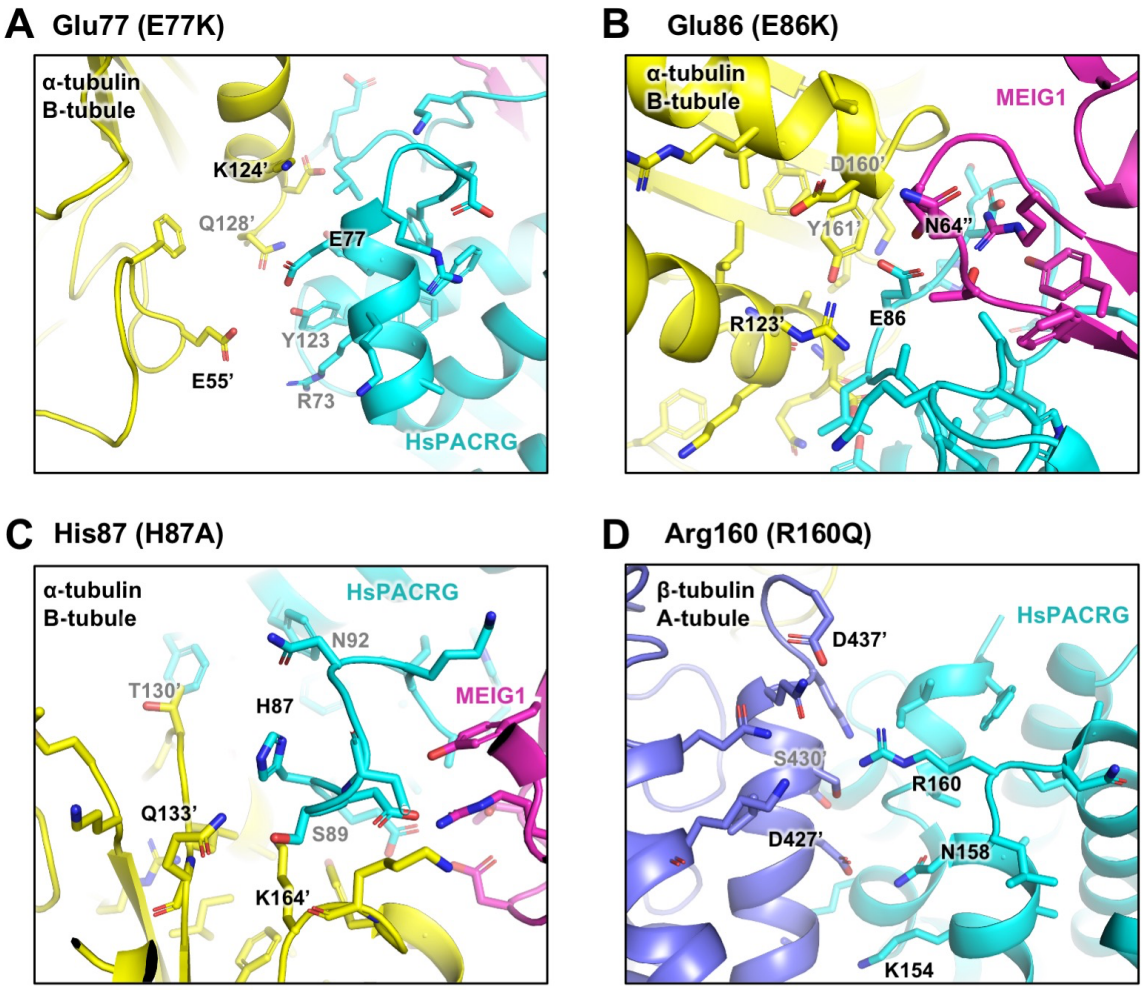

Supplemental Figure S8. **Critical sites for the interaction of human PACRG:MEIG1 with human tubulin in homology model of the axonemal doublet microtubule, related to Figure 3, 4, and 5.** PACRG residues are labeled with amino acid and number, tubulin residues are labeled additionally with a single prime (‘), MEIG1 residues with a double prime (“). **(A**) The mutation E77K enhances tubulin binding in our assays. In the model, Glu77 is adjacent to Glu55’ in α-tubulin (B-tubule). Thus the mutation E77K could lead to formation of a salt bridge. **(B)** The rare human variant E86K reduces tubulin binding. In the model, Glu86 is adjacent to Arg123’ in α-tubulin (B-tubule). The mutation E86K would break a salt bridge. **(C)** The mutation H87A reduces tubulin binding. The H87A mutation could break hydrogen bonds with Gln133’ or Lys164’. **(D)** The rare human variant R160Q dramatically reduces tubulin binding. Arg160 may interact with Asp427’ or Asp437’ in β-tubulin, and thus the R160Q mutation may break favorable interactions.

Supplemental Table S1. Evolution of PACRG-Parkin head-to-head (H2H) gene structure and conservation of PACRG and MEIG1, related to Figure 7.

Species name (latin)	Common name	PACRG-Parkin H2H?	Space (kb)	%ID PACRG	%ID MEIG1	Comments
Homo sapiens	Human	Yes	0	100.0	100.0	
Pan troglodytes	Chimp	Yes	0	100.0	97.7	
Gorilla gorilla	Gorilla	Yes	0	100.0	96.6	
Sus scrofa	Pig	Yes	240	96.9	94.3	
Rattus norvegicus	Rat	Yes	0	96.1	92.1	
Mus musculus	Mouse	Yes	0	92.1	87.5	
Ursus maritimus	Polar bear	Yes	200	97.3	95.5	
Myotis lucifugus	Little brown bat	Yes	0	90.0	90.9	
Gallus gallus	Chicken	Yes	0	70.4	77.0	
Calypte anna	Hummingbird	Yes	150	85.0	80.7	
Anolis carolinensis	Green anole	Yes	0	92.2	77.0	
Alligator mississippiensis	American alligator	Yes	0	81.4	81.8	
Terrapene mexicana triunguis	Three-toed box turtle	Yes	0	82.9	87.5	
Xenopus laevis	African clawed frog	n.a.	n.a.	90.0	75.0	No parkin/PINK1
Xenopus tropicalis	Tropical clawed frog	n.a.	n.a.	91.3	75.0	No parkin/PINK1
Danio rerio	Zebrafish	No	n.a.	89.6	71.6	
Callorhinchus milii	Elephant shark	Yes	0	76.8	79.5	
Salmo salar	Atlantic salmon	No	n.a.	88.7	75.3	
Aplysia californica	Sea slug	No	n.a.	82.3	61.0	
Drosophila melanogaster	Fruit fly	No	n.a.	59.9	none	No MEIG1
Caenorhabditis elegans	Nematode worm	No	n.a.	33.5	none	No MEIG1
Chlamydomonas reinhardtii	Green algae	n.a.	n.a.	63.7	none	No Parkin/PINK1, MEIG1
Tetrahymena thermophila	Ciliate	n.a.	n.a.	60.5	none	No Parkin/PINK1, MEIG1
Paramecium tetraurelia	Ciliate	n.a.	n.a.	58.7	none	No Parkin/PINK1, MEIG1
Trypanosoma brucei	Kinetoplastids	n.a.	n.a.	57.4	none	No Parkin/PINK1, MEIG1
Oxyrrhis marina	Dinoflagellate	n.a.	n.a.	None	38.9	No Parkin/PINK1, PACRG

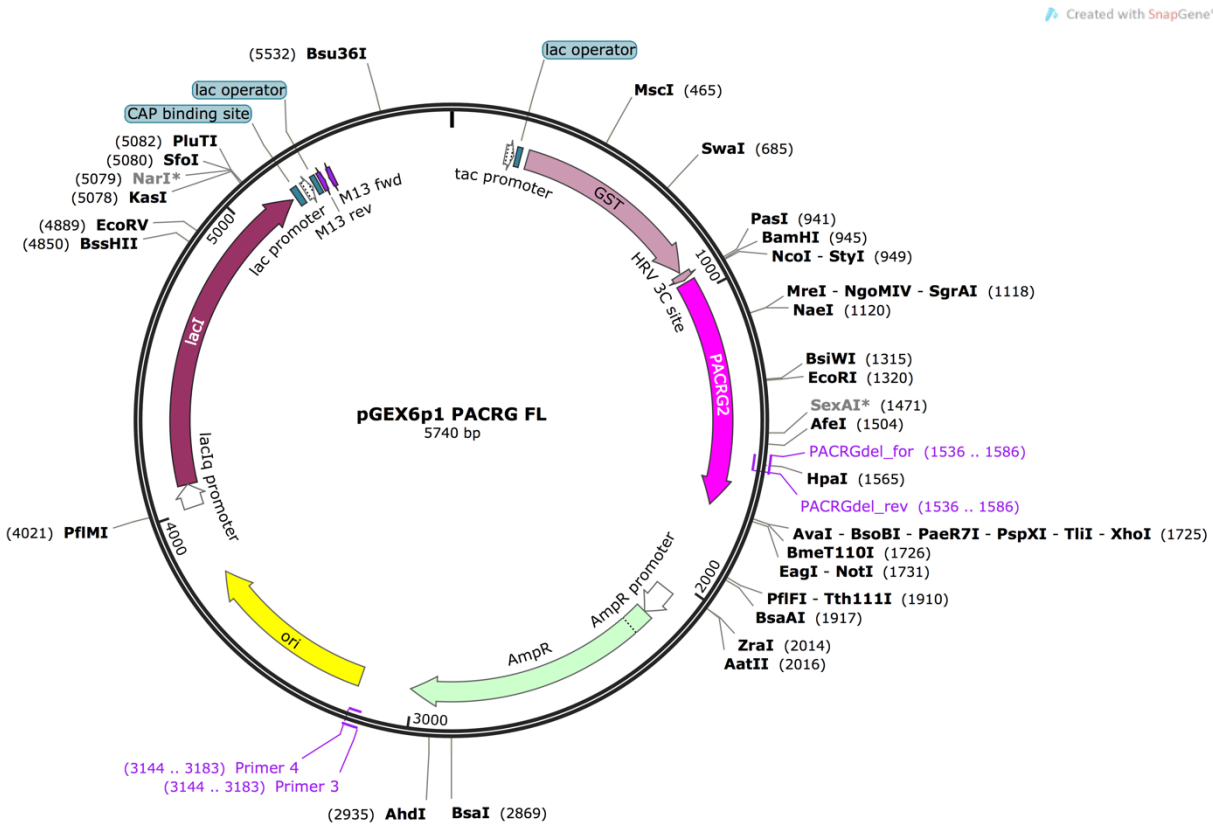

CC**ATG**GTTGCGGAAAAAGAAACCCTGTCTCTGAACAAATGCCCGGACAAAATGCCGAAAC
GTACCAAACTGCTGGCGCAGCAGCCGCTGCCGGTTCACCAGCCGCACTCTCTGGTTTCTG
AAGGTTTCACCGTTAAAGCGATGATGAAAAACTCTGTTGTTCGTGGTCCGCCGGCGGCGG
GTGCGTTCAAAGAACGTCCGACCAAACCGACCGCGTTCCGTAAATTCTACGAACGTGGTG
ACTTCCCGATCGCGCTGGAACACGACTCTAAAGGTAACAAAATCGCGTGGAAAGTTGAAAT
CGAAAAACTGGACTACCACCACTACCTGCCGCTGTTCTTCGACGGTCTGTGCGAAATGACC
TTCCCGTACGAATTCTTCGCGCGTCAGGGTATCCACGACATGCTGGAACACGGTGGTAAC
AAAATCCTGCCGGTTCTGCCGCAGCTGATCATCCCGATCAAAAACGCGCTGAACCTGCGT
AACCGTCAGGTTATCTGCGTTACCCTGAAAGTTCTGCAGCACCTGGTTGTTTCTGCGGAAA
TGGTTGGTAAAGCGCTGGTTCCGTACTACCGTCAGATCCTGCCGGTTCTGAACATCTTCAA
AAACATGAACGTTAACTCTGGTGACGGTATCGACTACTCTCAGCAGAAACGTGAAAACATC
GGTGACCTGATCCAGGAAACCCTGGAAGCGTTCGAACGTTACGGTGGTGAAAACGCGTTC
ATCAACATCAAATACGTTGTTCCGACCTACGAATCTTGCCTGCTGAAC**TAA**CTCGAG

Supplemental Data S1. **Vector map of pGEX6p1-PACRG short isoform (257 a.a.), related to the STAR Methods**. The sequence of the PACRG coding sequence (codon-optimized for E. coli expression), with the NcoI and XhoI restriction sites underlined, is shown below. The initiator (Met) and stop codons are in bold.

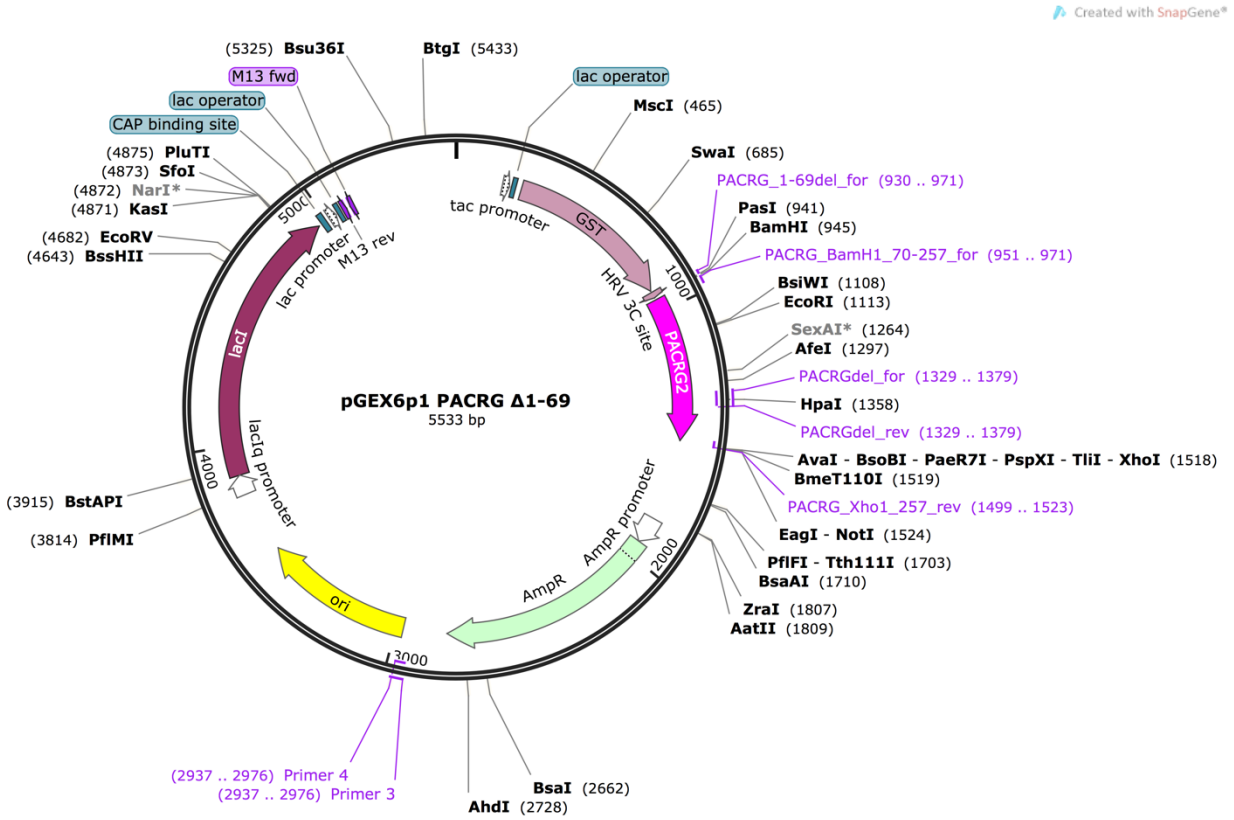

Supplemental Data S2. Vector map of pGEX6p1-PACRG$^{\Delta 1\text{-}69}$, related to the STAR Methods.

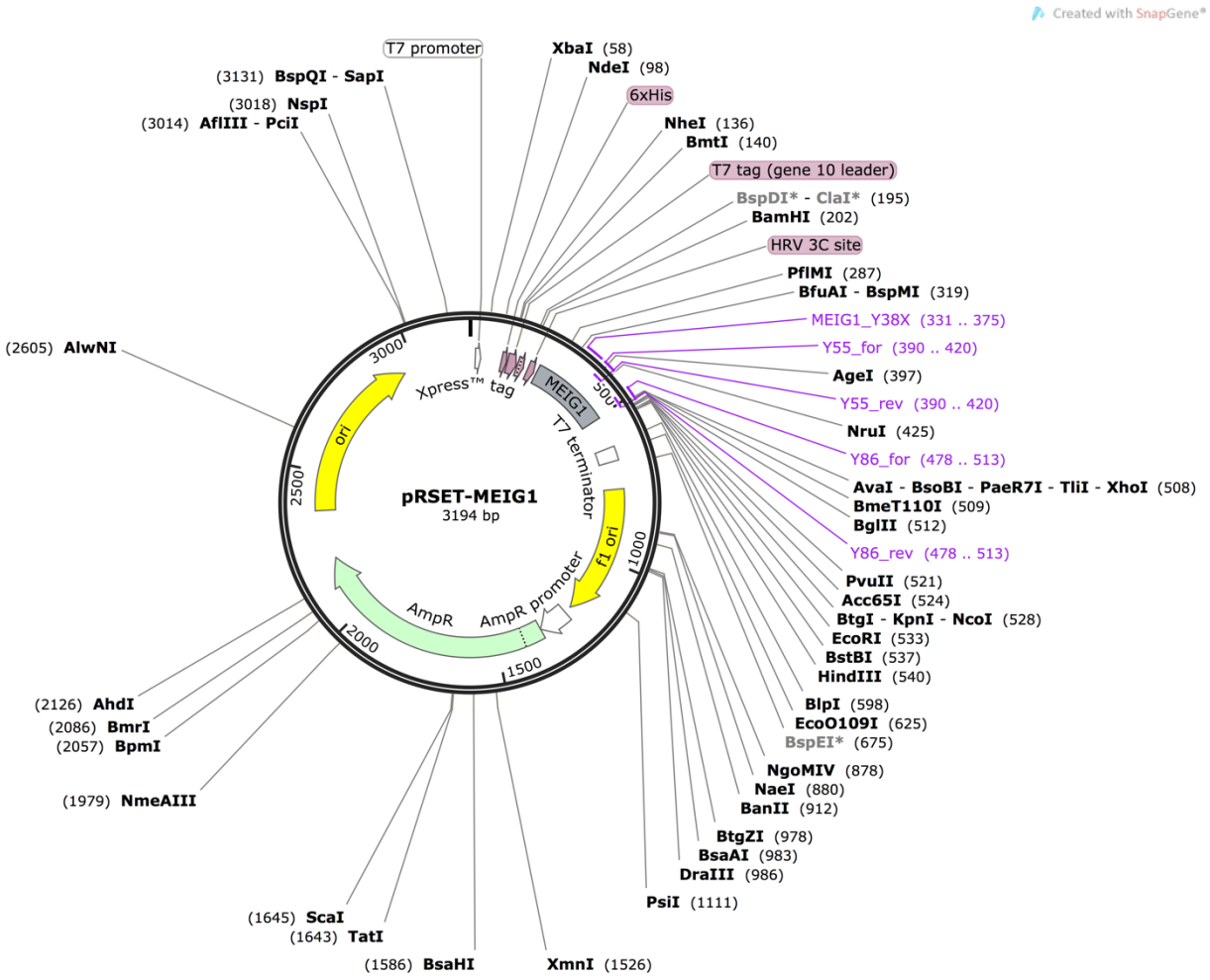

CAT**ATG**CGGGGTTCTCATCATCATCATCATCATGGTATGGCTAGCATGACTGGTGGACAGC
AAATGGGTCGGGATCTGTACGACGATGACGATAAGGATCGATGGGGATCCCTGGAAGTTC
TGTTTCAGGGTCCGCTGGGTAGCATGGCAAGCAGTGATGTTAAACCGAAAAGCGTTAGCC
ATGCCAAAAAATGGTCAGAAGAAATCGAAAACCTGTATCGTTTTCAGCAGGCAGGTTATCG
TGATGAAACCGAATATCGTCAGGTTAAACAGGTTAGCATGGTTGATCGTTGGCCTGAAACC
GGTTATGTTAAAAAACTGCAGCGTCGCGATAACACCTTCTACTATTACAATAAACAGCGCGA
GTGCGACGATAAAGAAGTGCATAAAGTTAAAATCTATGCCTAT**TAA**CTCGAG

Supplemental Data S3. Vector map of pRSET-His$_6$-MEIG1, related to the STAR Methods. The sequence of the open-reading frame comprising the His$_6$-tag (red), Nde1 and Xho1 sites (underlined) and codon-optimized sequence of MEIG1 (blue) is shown below. The initiator (Met) and stop codons are in bold.

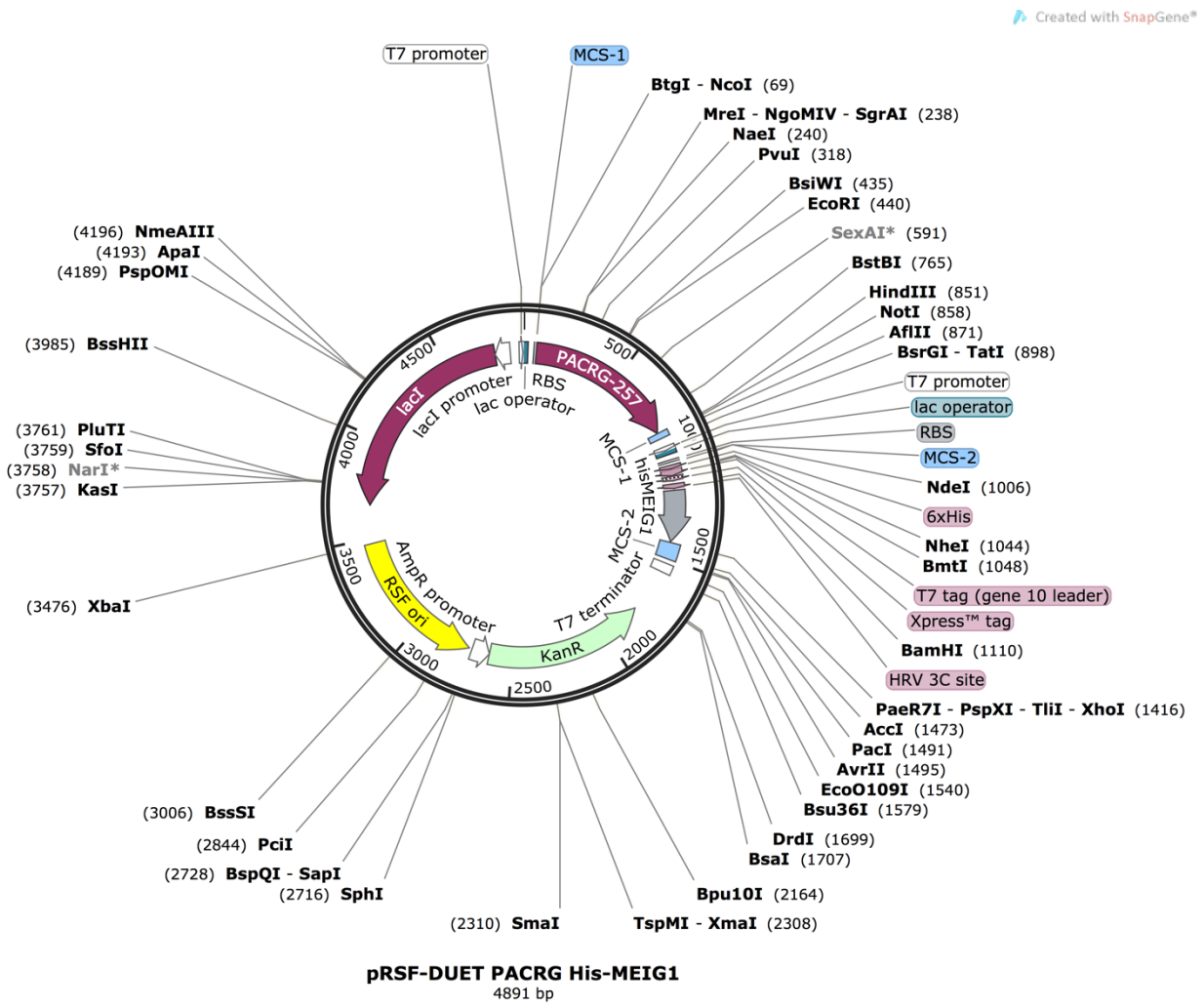

Supplemental Data S4. Vector map of pRSF-DUET PACRG^{FL}-His$_6$MEIG1, related to the STAR Methods.

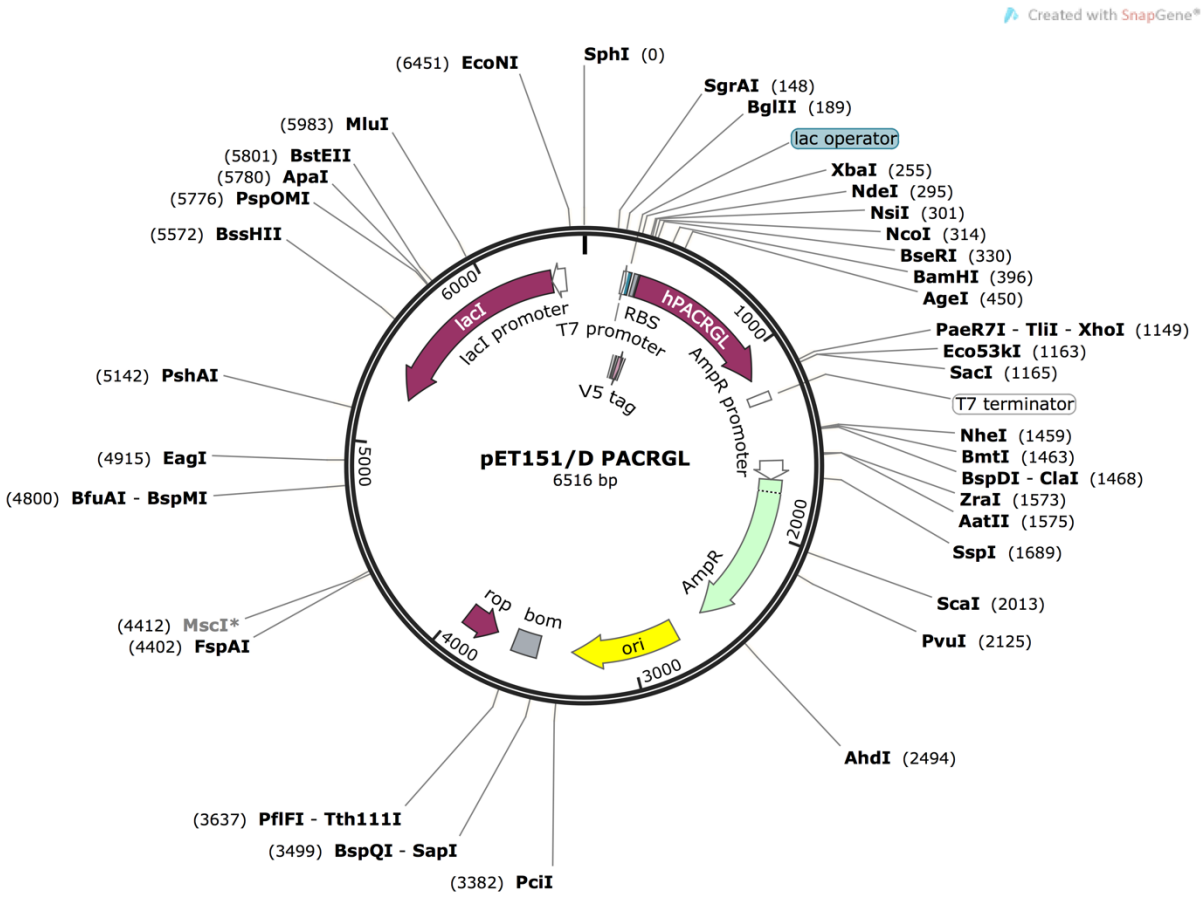

CAT**ATG**CATCATCACCATCACCATGGTAAGCCTATCCCTAACCCTCTCCTCGGTCTCGATT
CTACGGAAAACCTGTATTTTCAGGGAATTGATCCCTTCACCGGATCCATGCAGAAAAGCGA
AGGTAGCGGTGGCACCCAGCTGAAAAATCGTGCAACCGGTAATTATGATCAGCGTACCAG
CAGCAGTACACAGCTGAAACACCGTAATGCAGTTCAGGGTAGCAAAAGCAGCCTGAGCAC
CAGCAGTCCGGAAAGCGCACGTAAACTGCATCCGCGTCCGAGCGATAAACTGAATCCGAA
AACCATTAATCCGTTTGGTGAACAGAGCCGTGTTCCGAGCGCATTTGCAGCAATTTATAGC
AAAGGTGGTATTCCGTGTCGTCTGGTTCATGGTAGCGTTAAACATCGTCTGCAGTGGGAAT
GTCCGCCTGAAAGCCTGAGCTTTGATCCGCTGCTGATTACCCTGGCCGAAGGTCTGCGTG
AAACCAAACATCCGTATACCTTTGTTAGCAAAGAAGGTTTTCGCGAACTGCTGTTAGTTAAA
GGTGCACCGGAAAAAGCAATTCCGCTGTTACCGCGTCTGATTCCGGTTCTGAAAGCAGCA
CTGGTTCATAGTGATGATGAAGTTTTTGAACGTGGTCTGAATGCCCTGGTTCAGCTGAGCG
TTGTTGTTGGTCCGAGCCTGAATGATCATCTGAAACATCTGCTGACCAGCCTGAGTAAACG
TCTGATGGATAAAAAGTTTAAAGAGCCGATTACCAGCGCACTGCAGAAACTGGAACAGCAT
GGTGGTAGCGGTAGCCTGTCAATTATCAAAAGCAAAATTCCGACCTATTGCAGCATCTGCT
GTTAACTCGAG

Supplemental Data S5. Vector map of pET-151/D His$_6$-PACRGL, related to the STAR Methods. The sequence of the open-reading frame comprising the His$_6$-tag (red), Nde1 and Xho1 sites (underlined) and codon-optimized sequence of human PACRGL (blue) is shown below. The initiator (Met) and stop codons are in bold.